



ISSN NO. 2320-5407

Journal homepage: <http://www.journalijar.com>

INTERNATIONAL JOURNAL  
OF ADVANCED RESEARCH

## RESEARCH ARTICLE

EFFECT OF Ca DOPING ON STRUCTURAL, OPTICAL, MAGNETIC AND DIELECTRIC  
PROPERTIES OF BiFeO<sub>3</sub> NANOPARTICLES.

N. Manjula, s. Ramu, k. Sunil kumar, r.p.vijayalakshmi.

Department of Physics, Sri Venkateswara University, Tirupati 517 502, India.

**Manuscript Info****Manuscript History:**

Received: 14 January 2016

Final Accepted: 26 February 2016

Published Online: March 2016

**Key words:**Sol-Gel synthesis, BiCaFeO<sub>3</sub> material, electrical and dielectric analysis.**\*Corresponding Author**

r.p.vijayalakshmi.

**Abstract**

We proposed Sol-gel method to study the structure, optical, magnetic and dielectric properties of Bi<sub>1-x</sub>Ca<sub>x</sub>FeO<sub>3</sub> (x= 0.00, 0.01, 0.02, 0.03, 0.04 and 0.05) nano particles. The XRD spectrum exhibited predominant (012) and (110) orientation peaks at  $2\theta = 31.9^\circ$  and  $2\theta = 32.1^\circ$  corresponding to rhombohedral structure with R3c space group. From optical studies the band gap of BFO and Ca doped BFO nanoparticles were decreased from 2.13 to 1.96eV. The observed narrow band gap in the BFO system opens new vistas for the application of this material as multiferroic semiconductor. From magnetic properties the saturation magnetization for BFO (2.90 emu/gm) and for Ca doped BFO increased significantly from 1.00 emu/gm to 3.29 emu/gm. Dielectric and electric properties were studied over a frequency range of 10 Hz – 1 MHz. The dielectric constant was observed to decrease with increase in frequency. From cole-cole plots, as the Ca concentration increases, all semicircles become bigger and shift towards higher-frequency region, indicating a increment of grain and grain boundary resistance

Copy Right, IJAR, 2016.. All rights reserved

**Introduction:-**

Prime objectives of a synthetic approach is achieving rich functionality in a single material by combination of different physical properties. Multiferroics are such materials in which two or more of the primary ferroic properties are united in the same phase [1-3]. This class of materials has immense application in data storage, sensors, spin valves, spintronics, quantum electromagnets, microelectronic devices etc [4-8]. Bismuth ferrite is one of the rare multiferroic compounds in which ferroelectricity and magnetism coexist at room temperature. Both its anti ferromagnetic and ferroelectric transition temperatures are well above room temperature (643 K and 1100 K, respectively). It has been synthesized in bulk, thin film and nano form [9-14, 5].

Considerable attention has been devoted to this material because of its fundamental coupling phenomena of the multiple order parameters and practical applications for magneto electric devices based on electrically controlled magnetism [15–17]. Bulk BiFeO<sub>3</sub> (BFO) has a rhombohedral symmetry (space group R3c) and its ferroelectric polarization of  $\sim 100 \mu\text{C cm}^{-2}$  is oriented along one of the (111) pseudocubic axes [18–21]. The perovskite-type unit cell has a lattice parameter of  $a = 3.965 \text{ \AA}$  and a rhombohedral angle of around  $89.481^\circ$  at room temperature [5]. The polarization is mainly caused by the Bi<sup>3+</sup> lone pair ( $6s^2$  orbital), i.e. the polarization originates mostly from the A-site while the magnetization comes from Fe<sup>3+</sup>, i.e. the B-site. However, pure BFO has a serious high leakage current problem resulting from charge defects such as oxygen vacancies and the cancellation of ion magnetic moments due to its spatial periodic inhomogeneous spin structure, these factors hinders its practical applications in multiferroic devices. Considerable efforts have been expended to improve BFO properties; e.g., A-site substitution with La<sup>3+</sup>, Nd<sup>3+</sup>, Ce<sup>3+</sup> and Tb<sup>3+</sup> [22-27] and B-site substitution with Ni<sup>2+</sup>, Cu<sup>2+</sup>, Co<sup>2+</sup>, Cr<sup>3+</sup>, Mn<sup>3+</sup>, Ti<sup>4+</sup>, Zr<sup>4+</sup> and V<sup>5+</sup> [28-30] etc. These studies confirmed that ion doping is an effective method to improve BFO properties. Since ferroelectricity of BFO evolves from a lone pair of A-site Bi<sup>3+</sup> ion electrons [31-33], ferroelectric property effects are very important for many applications [34-35]. BFO with intermediate or mixed valance structure are gaining importance due to improvement in leakage current and multiferroic properties. The reports available on Ca doped

BFO are L.V.Costa et al. [36] studied the ferroelectric properties in Ca-doped BiFeO<sub>3</sub> using Polymeric Precursor Method (PPM). Recently, Zhu et al. [37] studied the structural and magnetic properties of BFO<sub>1-x</sub>(PbTiO<sub>3</sub>)<sub>x</sub> solid solutions.

To our knowledge no reports are available on Ca doped BiFeO<sub>3</sub> nanoparticles through sol-gel method. Hence we synthesized pure and Bi<sub>1-x</sub>Ca<sub>x</sub>FeO<sub>3</sub> (X = 0.00, 0.01, 0.01, 0.02, 0.03, 0.04 and 0.05) nano particles through a sol-gel process and obtained good dielectric and magnetic properties of the nanoparticles. This paper presents the synthesis, dielectric and magnetic properties of the Ca doped BiFeO<sub>3</sub> nanoparticles.

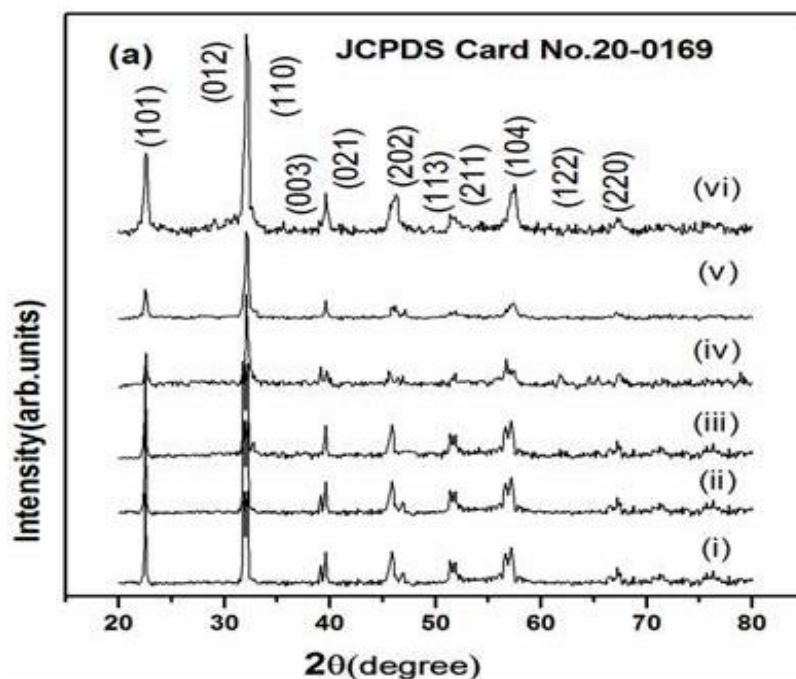
### Experimental:-

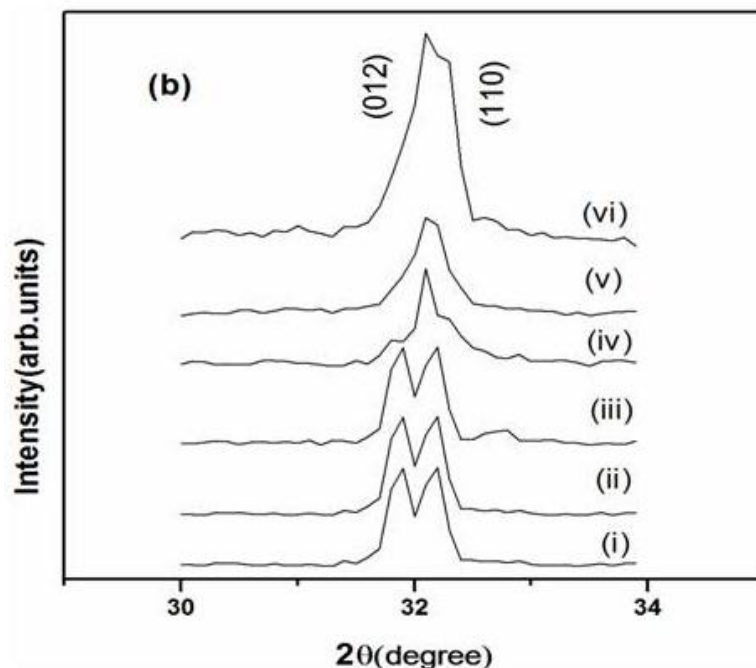
The reagents were of analytical grade and were used without further purification. Following is a typical procedure, Bismuth nitrate pentahydrate [Bi (NO<sub>3</sub>)<sub>3</sub>.5H<sub>2</sub>O], iron nitrate nonahydrate [Fe (NO<sub>3</sub>)<sub>3</sub>.9H<sub>2</sub>O] and Calcium nitrate polyhydrate Ca (NO<sub>3</sub>)<sub>2</sub>.4H<sub>2</sub>O were weighed in stoichiometric proportions and dissolved in deionized water to make a solution with an independent concentration of 0.2 M, to this mixer diluted nitric acid (65~68% HNO<sub>3</sub>) was added. Then Chelating agent tartaric acid was added in 1:1 metal ion ratio. The light-yellow-colored transparent solution was heated under vigorous stirring in the oven at 160°C for 4-5h. Subsequently powders were calcined in the oven at 600°C for 3h.

Crystalline structure of the Ca doped BiFeO<sub>3</sub> particles were obtained using an X-ray diffractometer (model-3003TT) with Cu K $\alpha$  radiation source (Wavelength,  $\lambda=1.5420$  Å) in the  $2\theta$  range of 20°-80° with a scan rate of 1°/min. The sample composition was obtained by Energy dispersive X-ray (EDAX) analysis. The particle size and structural studies has been carried out using transmission electron microscopy (TEM), and high-resolution TEM (HRTEM) of Hitachi-H7650. The band gap for all samples has been investigated by diffuse reflectance spectroscopy using JASCO V670 UV-Visible spectrometer in the range from 200-2000 nm. The magnetization of the BFO powders was carried out by using vibrating sample magnetometer (VSM) integrated in a physical property measurement system (PPMS-9, Quantum Design). Dielectric and conductivity studies were carried out using Impedance Analyzer (Model) solatron (SI 1260) General a.c circuit theory.

### Results and Discussion:-

#### Structural studies:-





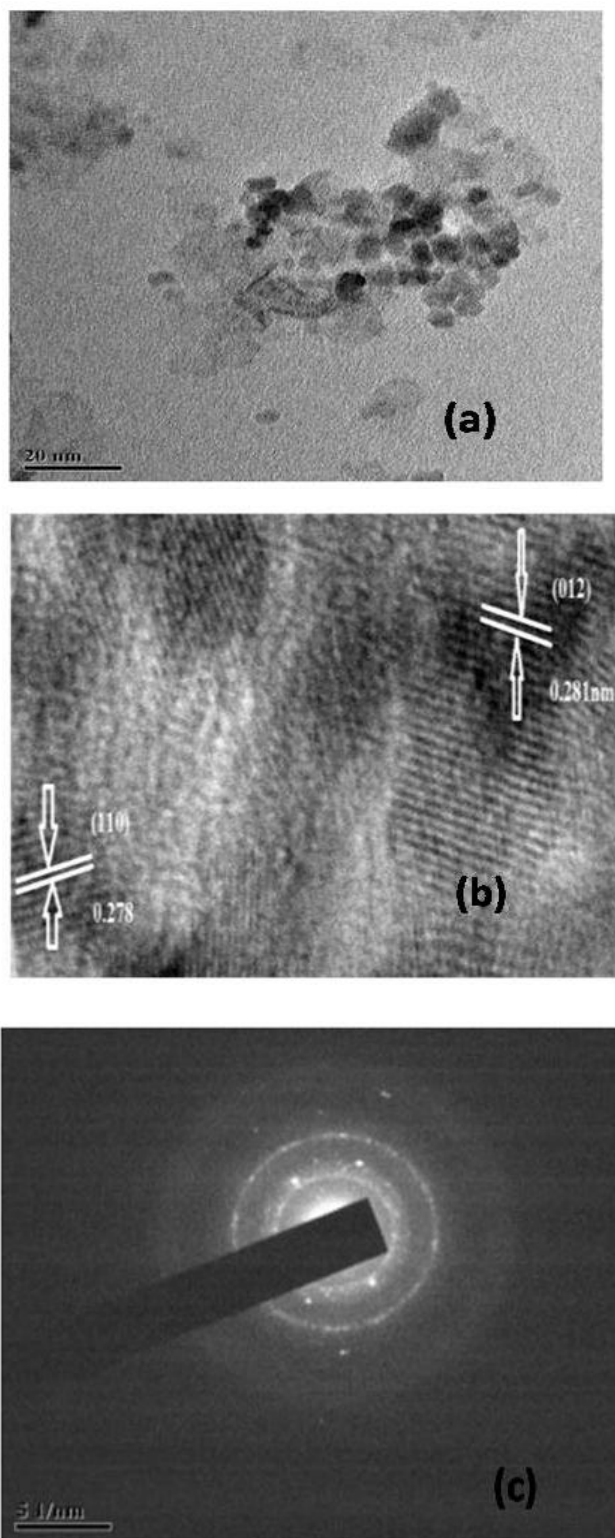
**Figure 1(a)** X-ray diffraction patterns for BiFeO<sub>3</sub> nanoparticles having different Ca concentration (i)  $x = 0.00$  (ii)  $x = 0.01$  (iii)  $x = 0.02$  (iv)  $x = 0.03$  (v)  $x = 0.04$  (vi)  $x = 0.05$ , **(b)** Change in the relative intensity of indicated twin peaks of (i)  $x = 0.00$  (ii)  $x = 0.01$  (iii)  $x = 0.02$  (iv)  $x = 0.03$  (v)  $x = 0.04$  (vi)  $x = 0.05$ .

Figure 1(a) shows the XRD patterns of BiFeO<sub>3</sub> and Ca doped BiFeO<sub>3</sub> nanoparticles. Observed XRD patterns could be indexed to rhombohedral structure of BiFeO<sub>3</sub> with space group R3c (JCPDS card number 20-0169), no other peaks (e.g., Fe<sub>2</sub>O<sub>3</sub>, Bi<sub>2</sub>O<sub>3</sub>, Bi<sub>2</sub>Fe<sub>4</sub>O<sub>9</sub> etc) are detected in the pure BFO nanoparticles confirmed the clean phase formation of the doped samples. With increasing Ca concentration, the splitting behavior of (012) and (110) peak was decreased gradually, it is observed from the magnified XRD pattern in the vicinity of  $2\theta$  around 32 degrees (Figure 1(b)). From Fig 1(b) we find the (012) and (110) separation of diffraction peaks for BCFO samples. In addition to that we can observe the merging of peaks with increasing Ca concentration, for  $x = 0.05$  the two peaks nearly merge into a single broad peak and such a merged peak also has a tendency to shift toward higher  $2\theta$  value. This result suggests that the rhombohedral structure is distorted by Ca substitution, which has been also observed in RE doped BFO ceramics [38-42]. Similar type of pattern was observed by B. Bhushan et al for 5 mol% of Ca, Sr and Ba ions.

**Table 1.** Lattice parameters, cell volume and grain size of BiFeO<sub>3</sub>: Ca nanoparticles sintered at 600 °C

S.NO	Bi <sub>1-x</sub> Ca <sub>x</sub> FeO <sub>3</sub>	a(A <sup>0</sup> )	c(A <sup>0</sup> )	c/a	Volume [Å] <sup>3</sup>	Grain size (nm)
1	X= 0.00	5.530	6.912	1.249	168.94	28
2	X= 0.01	5.538	6.906	1.247	169.67	26
3	X= 0.02	5.556	6.895	1.240	171.33	25
4	X= 0.03	5.569	6.852	1.230	172.54	12
5	X= 0.04	5.571	6.776	1.216	172.72	9
	X=0.05	5.5667	6.771	1.215	172.32	8

The average crystallite sizes of our samples was calculated using Scherrer formula  $D_p = 0.94\lambda/\beta\cos\theta$ , where  $\lambda$  is the X-ray wavelength,  $\beta$  is the full width at half maximum of the intensity peak at the diffraction angle  $\theta$  were noted to be around 28 nm for BiFeO<sub>3</sub> while for all the five doped samples it reduced to 8 nm. Lattice parameters a and c were calculated by using the relation  $\sin^2\theta = \lambda^2/3a^2(h^2+hk+K^2) + \lambda^2l^2/4c^2$ , where  $\theta$  is Bragg angle [43]. The strong peaks (012) and (110) were employed for such calculations. The grain size and lattice parameters are shown in Table 1 which are in good agreement with values reported for related compounds [44-48]. Further, it is evident from Table 1 that crystallite size and lattice parameter decrease with the increase in Ca<sup>2+</sup> concentration.



**Figure 2** (a) TEM micrograph of Ca doped BiFeO<sub>3</sub> nanoparticle (b) HRTEM image of Ca doped BiFeO<sub>3</sub> nanoparticle (c) the corresponding SAED pattern.

The morphology of the BFO nanoparticles was examined by using TEM. Typical TEM images of Ca doped BFO powders calcined at 600°C for 3h are shown in Figure 2(a). It is revealed that the synthesized material consists of

nanoparticles with size distribution ranging from 16 to 6 nm. The microstructure of the powders appeared as spherical particles. Gurmeet singh [49] have reported the particle size between 30-26nm.

Figure 2(b) shows the high-resolution TEM (HRTEM) image of the Ca doped BiFeO<sub>3</sub> nanoparticles as well as selected area electron diffraction (SAED) (Figure 2(c)). SAED pattern taken from the nanoparticles, revealing the single crystalline nature and also sharp diffraction spots as visible from SAED pattern confirms the formation of well crystalline Ca doped BiFeO<sub>3</sub> nanoparticles. All the patterns can be indexed with space group R3c and lattice parameters of  $a=b=5.571 \text{ \AA}$  and  $c=6.776 \text{ \AA}$  are in good agreement with the XRD result. Extensive electron diffraction experiments identify unambiguously that almost all the BiFeO<sub>3</sub> and Ca doped BiFeO<sub>3</sub> nanoparticles are well crystallized and are of a single rhombohedrally distorted perovskite structure. The presence of (021) and (110) plane diffraction fringes in a sample with d-spacings of  $2.803 \text{ \AA}$  and  $2.785 \text{ \AA}$  are shown in Figure 2(b). This is also well matched to JCPDS Card No.20-0169. The corresponding SAED pattern is shown in Figure 2(c).

### Compositional Analysis:-

The Energy Dispersive X-ray Spectrometer (EDAX) analysis of all the six samples are shown in the following Figure 8 (a), (b), (c), (d), (e) & (f). The EDAX plot reveals no extra peaks related to elements other than the constituents. All the samples show the exact match for standard peak position for Bi, Fe, Ca and O. This reveals that the elemental composition of all the samples does not contain any foreign elements and if any parasitic phases are there, it has to be some form of Bi, Fe, Ca, and O only. The EDAX pattern exhibits an increase in the Ca signal at 3.6 KeV, which indicates the formation of a Ca-doped BFO material

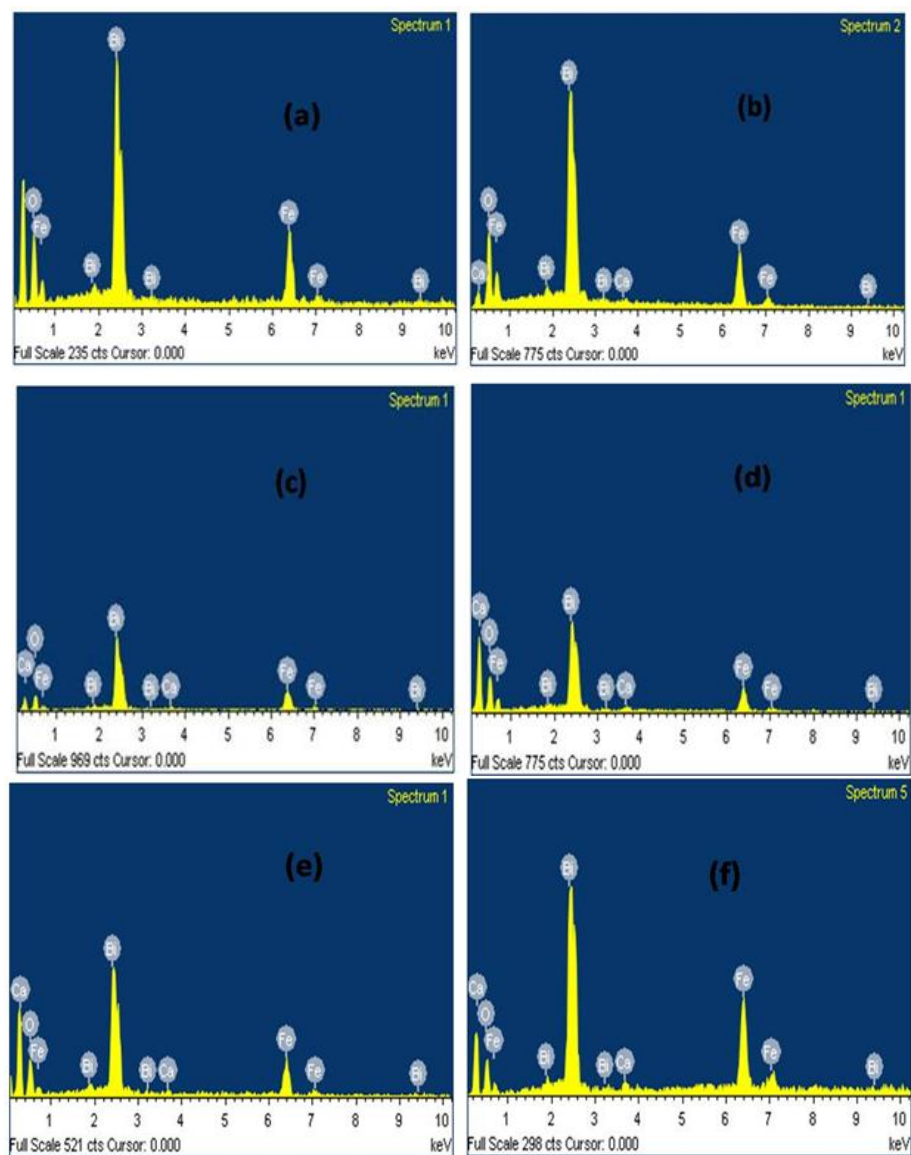


**Figure 3.2** EDAX spectrum of  $\text{Bi}_{1-x}\text{Ca}_x\text{FeO}_3$  (a)  $x = 0.00$  (b)  $x = 0.01$  (c)  $x = 0.02$  (d)  $x = 0.03$  (e)  $x = 0.04$  (f)  $x = 0.05$ .

### Band gap studies:-

- **3.3.1 UV-vis diffuse reflectance spectroscopy:-**

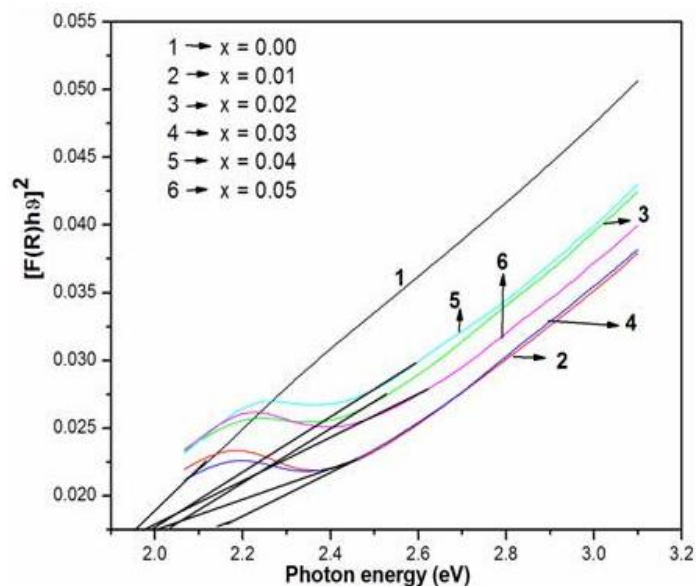


**Figure 3.3.1** Plots of  $[F(R)h\nu]^2$  versus  $h\nu$  for all six samples.

It is well known that the properties of diffuse reflectance spectra by semiconductors are relevant to the electronic structure features and hence are the key factors in determining their band gaps. The DRS spectra of sintered samples at  $600^\circ\text{C}$  are recorded and the band gap values were calculated by plotting the square of the Kubelka–Munk function [50]  $(F(R))^2$  versus energy and extrapolating the linear part of the curve to  $F(R)^2 = 0$ , as shown in figure 3.3.1. The band gap of BFO nanoparticles is  $\sim 1.96$  eV, which is in agreement with the earlier reported values similar to our work [51-53]. And with the increasing of Ca content, the value of band gap decreases from  $\sim 2.13$  eV for BCFO-5 to  $\sim 1.98$  eV for BCFO-1 nanoparticles. Similar trend of band gap variation with dopant can be seen in  $\text{Ca}^{2+}$  doped BFO nanoparticles [54].

### Magnetic Properties:-

The magnetic properties of Ca doped  $\text{BiFeO}_3$  was carried by using VSM. From Figure 3.4(a) it is observed that all hysteresis loops are symmetrical. The coercive field, remanent magnetizations are tabulated in Table 2. It should be noted that saturation in all M-H loops are easily achieved at an applied field of 15kOe.

The M-H curves in enlarged scale in the low magnetic field region are displayed in Figure 3.4(b) for different concentrations of Ca doped  $\text{BiFeO}_3$  nanoparticles. Unlike the magnetization reports [55] on bulk  $\text{BiFeO}_3$ , nanoparticles of  $\text{BiFeO}_3$  and Ca doped  $\text{BiFeO}_3$  show ferromagnetic ordering. The ferromagnetic property in our doped undoped nanoparticles may be originated for two reasons. Firstly, the canting of spin arrangement and secondly, the suppression of spiral spin arrangement. The presence of spiral spin arrangement of order 62nm is responsible for the suppression of magnetization in bulk BFO. But BFO nanoparticles having particle size of the order of this spiral spin structure leads to non exact compensation of antiferromagnetic ordering hence exhibit room temperature ferromagnetism as observed in our nanoparticles [56]. The largest value of the  $M_s$  obtained for  $\text{Bi}_{0.95}\text{Ca}_{0.05}\text{FeO}_3$  sample is  $\sim 3.29$  emug $^{-1}$ . This value of  $M_s$  for Ca doped BFO is even larger than some of the ferro or paramagnetic metal ions doped BFO samples [57, 55 and 58]. As this divalent metal ion ( $\text{Ca}^{2+}$ ) get substituted in the system at Bi site a sort of charge imbalance could be arise, which may destabilize the BCFO, to maintain the electro neutrality, one oxygen vacancy would be created for every two alkali earth ions introduced into the BFO lattice. Thus created oxygen vacancies may contribute to the enhanced magnetic properties of the doped BFO samples as established by Rao and co-workers [59]. This high value of saturation magnetization observed in  $x = 0.05$  may also be due to the lower particle size. The observation of higher coercivity and saturation magnetization in

some of the doped nanoparticles may help in finding a way for improving magnetization in  $\text{BiFeO}_3$  that in turn, will lead to many technological applications.

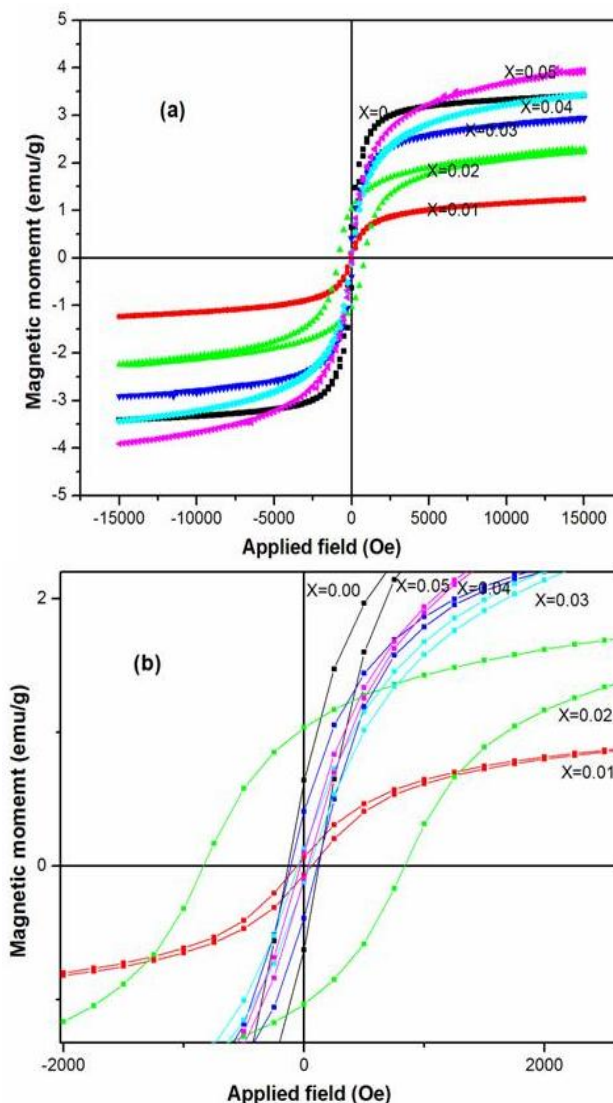


**Figure 3.4(a)** M–H hysteresis loops of  $\text{Bi}_{1-x}\text{Ca}_x\text{FeO}_3$  ( $x=0.00, 0.01, 0.02, 0.03, 0.04, 0.05$ ) nanoparticles, **(b)** Magnified M–H hysteresis loops of  $\text{Bi}_{1-x}\text{Ca}_x\text{FeO}_3$  ( $x=0.00, 0.01, 0.02, 0.03, 0.04, 0.05$ ) nanoparticles.

**Table 2:-**

Sample $\text{Bi}_{1-x}\text{Ca}_x\text{FeO}_3$	Grain Size (nm)	Coercive field (kOe)	Remenant magnetization ( $\text{emu g}^{-1}$ )	Saturation magnetization ( $\text{emu g}^{-1}$ )
X = 0.00	28	124	0.642	2.90
X = 0.01	26	62	0.067	1.00
X = 0.02	25	836	1.036	2.23
X = 0.03	12	109	0.407	2.47
X = 0.04	9	45	0.128	2.76
X = 0.05	8	30	0.100	3.29

## Dielectric Properties:-

### • 3.5.1 Dielectric Analysis:-

Figure 3.5.1 shows the frequency dependence of the dielectric constant and dielectric loss of the  $\text{Bi}_{1-x}\text{Ca}_x\text{FeO}_3$  ( $x=0, 0.01, 0.02, 0.03, 0.04$ ) samples at  $150^\circ\text{C}$  temperature. It has been observed that all the samples represent a decreasing trend in both  $\epsilon'$  and  $\tan \delta$  with increasing frequency from 10 Hz to 1 MHz. The dielectric constant is much higher at lower frequencies and its value decreases with increasing frequency of the applied alternating field. At higher frequencies, the dielectric constant shows no change and become frequency independent. The above variation of  $\epsilon'$  can be understood on the basis of Maxwell-Wagner model related to interfacial space charge relaxation [60-61]. The decrease in value of  $\epsilon'$  with frequency also indicates the existence of polarization originating from domain switching [62].

The space charges originate from oxygen ( $\text{V}_0^{2+}$ ) and bismuth ( $\text{V}_{\text{Bi}}^{3-}$ ) vacancies that follow the applied electric field at low frequencies and contribute to the dielectric constant. However at elevated frequency  $f > 1$  KHz, the weak dependence of  $\epsilon'$  and  $\tan \delta$  was observed, this account for the fact that at higher frequency electric domain rather than dipole of charged defect ( $\text{V}_0^{2+}$ ,  $\text{V}_{\text{Bi}}^{3-}$ , and  $\text{Fe}^{2+}$ ) mainly contribute to the characteristic of  $\epsilon'$  and  $\tan \delta$ . Moreover, the higher values of  $\tan \delta$  in BFO material generally represent large leakage current due to higher conductivity.

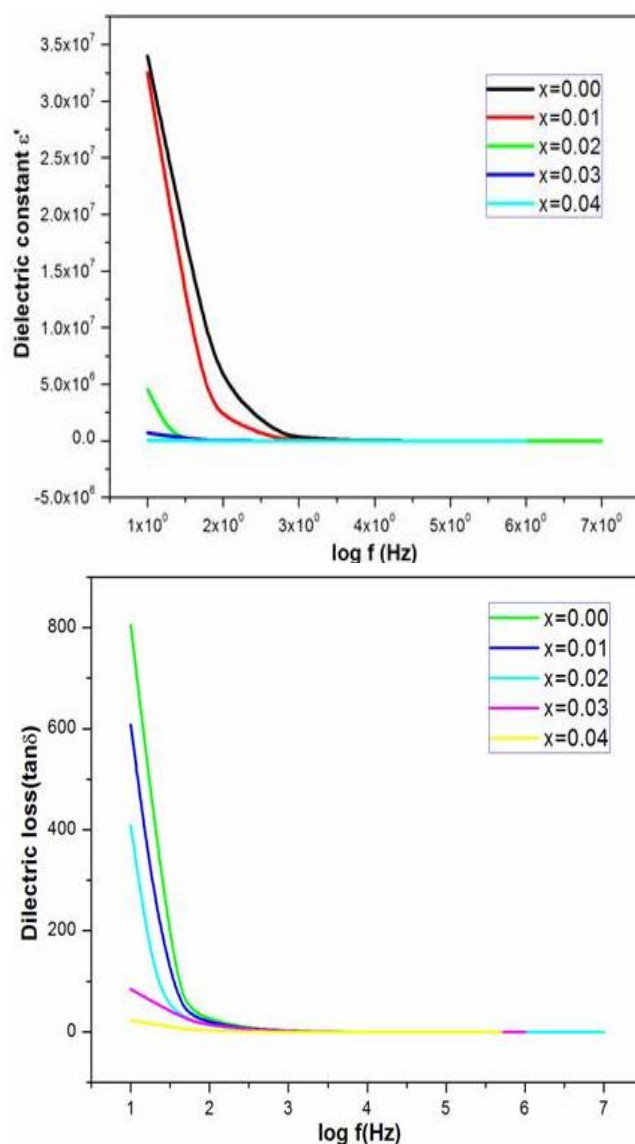


**Fig. 3.5.1** Frequency dependent dielectric constant ( $\epsilon'$ ) and dielectric loss ( $\tan \delta$ ) of  $\text{Bi}_{1-x}\text{Ca}_x\text{FeO}_3$  ( $x=0, 0.01, 0.02, 0.03, 0.04$ ) nanoparticles.

• 3.5.2 Electrical analysis:-

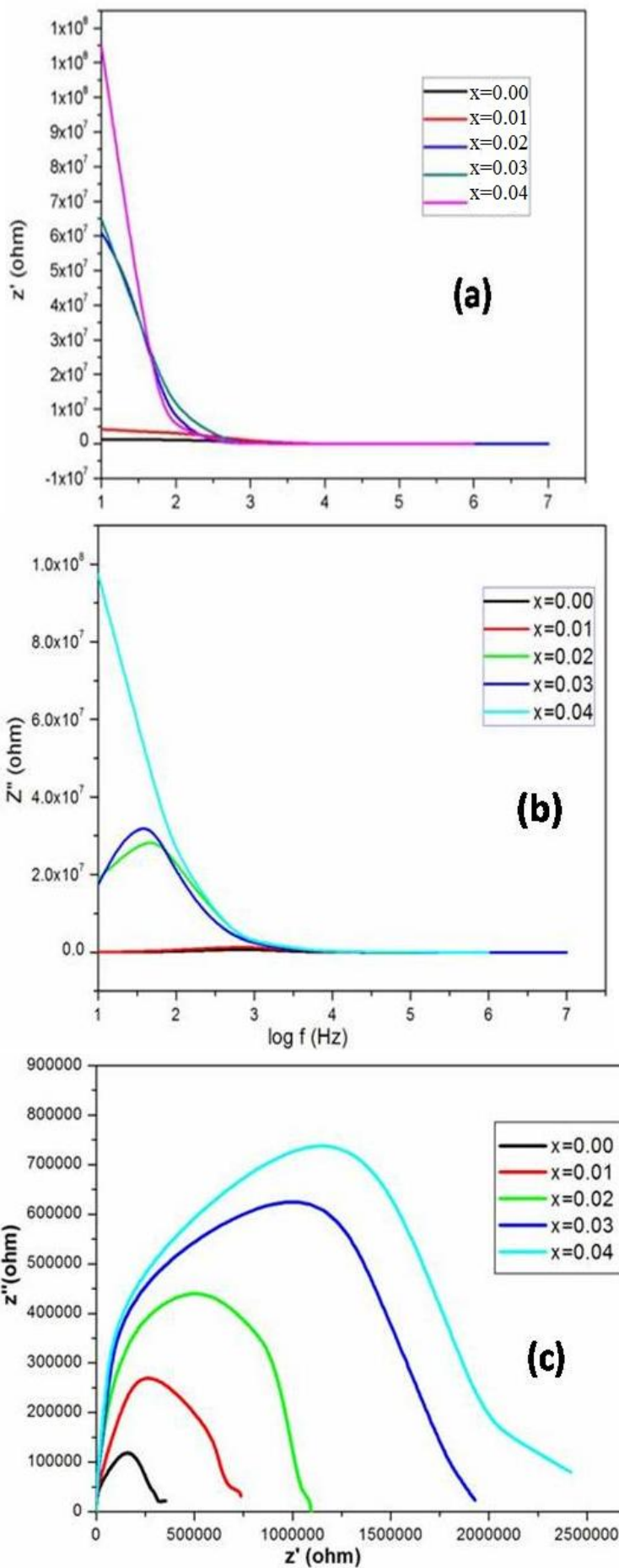


**Fig.3.5.2 (a)** Real part of impedance with respect to frequency for different concentrations of Ca doped BiFeO<sub>3</sub>, **(b)** Imaginary part of impedance with respect to frequency for different concentrations of Ca doped BiFeO<sub>3</sub>, **(c)**. Cole-cole plots of Bi<sub>1-x</sub>Ca<sub>x</sub>FeO<sub>3</sub> (x=0.00, 0.01, 0.02, 0.03, 0.04) at 150°C temperature

The response of the real components of impedance ( $Z'$ ) with frequency at room temperature for different concentration of Ca doped BiFeO<sub>3</sub> is shown in Fig.3.5.2 (a). At higher frequencies  $> 10^3$  Hz,  $Z'$  is almost independent of frequency,  $Z'$  considerably increases as frequency increases. This indicates that the components of capacity and resistance of the equivalent circuit are active in this range of frequencies and a increase in the total resistance of the sample. Fig.3.5.2 (b). Shows the variation of imaginary component of impedance ( $Z''$ ) with frequency for different concentration of Ca doped BiFeO<sub>3</sub>. The relaxation or Maxwell-Wagner type peaks in the low frequency region and the peak intensity is found to increase as the Ca concentration increases.

Figure 3.5.2(c) these plots allow the resistances related to grain interiors, grain boundaries, and sample/electrode interfaces to be separated because each of them has different relaxation time, resulting in separate semicircles in the complex impedance plane. The relaxation frequency for the grain interiors is one or two orders of magnitude higher than the relaxation frequency for grain boundaries, and the relaxation frequency resulting from the electrode process is much smaller than relaxation frequency of grain boundaries [63]. The observed semicircular arc at higher frequencies is attributed to the electrical properties of a parallel combination of bulk resistance and capacitance of the Bi<sub>1-x</sub>Ca<sub>x</sub>FeO<sub>3</sub> (x=0.00, 0.01, 0.02, 0.03, 0.04) samples. As the Ca concentration increases, all semicircles become bigger and shift towards higher-frequency region, indicating a increment of grain and grain boundary resistance. This explains the increase in  $Z'$  and  $Z''$  in Figs. 3.5. 2 (a) and (b) [64].

### Conclusions:-

BFO and BCFO were synthesized by sol-gel method. The effects of Ca doping on the variations of the structural, optical, magnetic and dielectric properties for BFO and BCFO were experimentally studied. XRD and TEM measurements confirmed the formation of pure and Ca doped BCFO nanoparticles. From optical studies the band gap was found to be ~1.96 eV for the pure sample whereas the band gap measured for doped samples was decreased from 2.13 to 1.98eV. The observed narrow band gap in the BFO system opens new vistas for the application of this material as multiferroic semiconductor. From magnetic properties the BFO and Ca doped BFO nanoparticles exhibit ferromagnetic behavior. The saturation magnetization for BFO (2.90 emu/gm) and for Ca doped BFO increased significantly from 1.00 emu/gm to 3.29 emu/gm. The dielectric constant was observed to decrease with increase in frequency. From cole-cole plots, As the Ca concentration increases, all semicircles become bigger and shift towards higher-frequency region, indicating a increment of grain and grain boundary resistance.

### Acknowledgements:-

Authors would like to thank RGNF (Rajiv Gandhi National Fellowship), New Delhi for providing financial assistance.

### References:-

- [1] Eerenstein, W.; Mathur, N.D.; Scott, J.F.; Nature, Rev., **2006**, 442, 759.  
DOI: 10.1038/nature05023
- [2] Catalan, G.; Scott, J.F.; Adv. Mater. **2009**, 21, 2463.  
DOI: 10.1002/adma.200802849
- [3] Bhushan, B.; Mukherjee, S.; Basumallick, A.; Bandopadhyay, S.; Das, D.; Hyperfine Interact. **2008**, 187,101  
DOI: 10.1007/s10751-008-9889-0
- [4] Rivera, J.V.; Schmid, H.; Ferroelectrics.**1997**, 204, 23.  
DOI: 10.1080/00150199708222185
- [5] Wang, J.; Neaton, J.B.; Zheng, H.; Nagarajan, V.; Ogale, S.B.; Liu, B.; Viehland, D.; Vaithyanathan, V.; Schlom, D.G.; Waghmare, U.V.; Spaldin, N.A.; Rabe, K.M.; Wuttig, M.; Ramesh, R.; Science. **2003**, 299, 1719.  
DOI: 10.1126/science.1080615
- [6] Bea, H.; Bibes, M.; Sirena, M.; Herranz, G.; Bouzehouane, K.; Appl. Phys. Lett.**2006**, 88, 062502.  
DOI: 10.1063/1.2170432
- [7]. Lin, Y-H.; Jiang, Q.; Wang, Y.; Nan, C-W.; Chen, L.; Yu, J.; Appl. Phys. Lett. **2007**, 90, 172507.  
DOI: 10.1063/1.2732182

- [8] Wang, Y.; Nan, C-W.; Appl. Phys. Lett. **2006**, 89, 052903.  
**DOI:**10.1063/1.2222242
- [9] Catalan, G.; Scott, J.F.; Adv. Mater. **2009**, 21, 2463.  
**DOI:** 10.1002/adma.200802849
- [10] Scott, J.F.; Singh, M.K.; Katiyar, R.S.; J.Phys. Condens. Matter **2008**, 20.  
**DOI:**10.1088/0953-8984/20/42/425223
- [11] Singh, M.K.; Katiyar, R.S.; Scott, J.F.; J.Phys.; Condens. Matter **2008**, 20, 252203.  
**DOI:**10.1088/0953-8984/20/25/252203
- [12] Singh, M.K.; Prellier, W.; Singh, M.P.; Katiyar, R.S.; Scott, J.F. Phys. Rev.B. **2008**, 77, 144403.  
**DOI:** 10.1103/PhysRevB.77.144403
- [13] Chu, Y.H.; Martin, L.W.; Holcomb, M. B.; Ramesh, R.; Mater. Today. **2007**, 10, 16.  
**DOI:** 10.1016/S1369-7021(07)70241-9
- [14] Zhao, T.; Scholl, A.; Zavaliche, F.; Lee, K.; Barry, M.; Doran, A.; Cruz, M. P.; Chu, Y.H.; Ederer, C.; Spaldin, N. A.; R. R.; Kim, D. M.; Baek, S. H.; Eom, C.B.; Ramesh, R.; Nat. Mater. **2006**, 5, 823.  
**DOI:** 10.1038/nmat1731
- [15] Ramesh, R.; Spaldin, N. A.; Nat. Mater. **2007**, 6, 21.  
**DOI:** 10.1038/nmat1805
- [16] Ishiwara, H.; Curr. Appl. Phys. **2012**, 12, 603.  
**DOI:** 10.1016/j.cap.2011.12.019
- [17] Martin, L.W.; Crane, S.P.; Chu, Y.-H.; Holcomb, M. B.; Gajek, M.; Huijben, M.; Yang, C.-H.; Balke, N.; Ramesh, R.; J. Phys.: Condens. Matter. **2008**, 20 (43), 434220.  
**DOI:**10.1088/0953-8984/20/43/434220
- [18] Roginska, Y. E.; Tomashpo Y. Y.; Venevtse, Y. N.; Petrov, V. M.; Zhdanov G. S.; Sov. Phys. JETP, **1966**, 23, 47.
- [19] Kiselev, S. V.; Ozerov, R. P.; Zhdanov, G. S.; Sov. Phys. Dokl. **1963**, 7, 742.
- [20] Teague, J. R.; Gerson, R.; James, W. J.; Solid State Commun., **1970**, 8(13), 1073.
- [21] Filipeev, V. S.; Smolyaninov, I. P.; Fesenko, E. G.; Belyaev, I. I.; Sov. Phys. Crystallogr. **1960**, 5, 913.
- [22] Huang, F.Z.; Lu, X.M.; Lin, W.W.; Wu, X.M.; Kan, Y.; Zhu, J.S.; Appl. Phys. Lett. **2006**, 89, 242914.  
**DOI:** 10.1063/1.2404942.
- [23] Yu, B.F.; Li, M.Y.; Liu, J.; Guo, D.Y.; Pei, L.; Zhao, X.Z.; J. Phys. D Appl. Phys. **2008**, 41, 065003.  
**DOI:**10.1088/0022-3727/41/6/065003
- [24] Wang, Y.; Nan, C.W.; J. Appl. Phys. **2008**, 103, 024103.  
**DOI:** 10.1063/1.2831026
- [25] Liu, J.; Li, M.Y.; Pei, L.; Yu, B.F.; Guo, D.Y.; Zhao, X.Z.; J. Phys. D Appl. Phys. **2009**, 42, 115409.  
**DOI:**10.1088/0022-3727/42/11/115409
- [26] Liu, J.; Li, M.Y.; Pei, L.; Wang, J.; Yu, B.F.; Wang, X.; Zhao, X.Z.; J. Alloys Compd. **2010**, 493, 544.  
**DOI:**10.1016/j.jallcom.2009.12.152
- [27] Lahmar, A.; Habouti, S.; Dietze, M.; Solterbeck, C.-H.; Es-Souni, M.; Appl. Phys.Lett. **2009**, 94, 012903.  
**DOI:** 10.1063/1.3064954
- [28] Wang, Y.; Nan, C.W.; Ferroelectrics. **2007**, 357, 172.  
**DOI:** 10.1080/00150190701542844
- [29] Naganuma, H.; Miura, J.; Okamura, S.; Appl. Phys. Lett. **2008**, 93, 052901.  
**DOI:** 10.1063/1.2965799
- [30] Kharel, P.; Talebi, S.; Ramachandran, B.; Dixit, A.; Naik, V.M.; Sahana, M.B.; Sudakar, C.; Naik, R.; Rao, M.S.R.; Lawes, G.; J. Phys. C Condens. Matter. **2009**, 21, 036001.  
**DOI:**10.1088/0953-8984/21/3/036001
- [31] Martin, L.W.; Crane, S.P.; Chu, Y.H.; Holcomb, M.B.; Gajek, M.; Huijben, M.; Yang, C.H.; Balke, N.; Ramesh, R.; J. Phys. C Condens. Matter. **2008**, 20, 434220.  
**DOI:**10.1088/0953-8984/20/43/434220
- [32] Catalan, G.; J.F. Scott, Adv. Mater. **2009**, 21, 2463.  
**DOI:** 10.1002/adma.200802849
- [33] Wang, K.F.; Liu, J.M.; Ren, Z.F.; Adv. Phys. **2009**, 58, 321.  
**DOI:** <http://dx.doi.org/10.1080/00018730902920554>
- [34] Liu, J.; Li, M.Y.; Pei, L.; Wang, J.; Hu, Z.Q.; Wang, X.; Zhao, X.Z.; Europhys. Lett. **2010**, 89, 57004.  
**DOI:** 10.1209/0295-5075/89/57004
- [35] Yuan, G.L.; Or, S.W.; J. Appl. Phys. **2006**, 100, 024109.

**DOI:** 10.1063/1.2220642

[36] Costa L.V. et al. *Materials Chemistry and Physics* **2014**, 144, 476.

[37] W.-M. Zhu, H.-Y. Guo, and Z.-G. Ye.; *Phys.Rev.B.* **2008**, 78, 014401.

**DOI:** 10.1103/PhysRevB.78.014401

[38] Zhang, S. T.; Zhang, Y.; Lu, M. H.; Du, C. L.; Chen, Y. F.; Liu, Z. G.; Zhu, Y. Y.; Ming, N. B.; Pan, X. Q. *Appl. Phys. Lett.* 2006, 88, 162901.

**DOI:** 10.1063/1.2195927

[39] Yuan, G. L.; Or, S. W.; Liu, J. M.; Liu, Z. G. *Appl. Phys. Lett.* **2006**, 89, 052905.

**DOI:** 10.1063/1.2266992.

[40] Yuan, G. L.; Or, S. W. *J. Appl. Phys.* **2006**, 100, 024109.

**DOI:** 10.1063/1.2220642.

[41] Liu, J.; Fang, L.; Zheng, F.G.; Ju, S.; Shen, M. R.; *Appl. Phys. Lett.* **2009**, 95, 022511.

**DOI:** 10.1063/1.3183580

[42] Kan, D.; Palova, L.; Anbusathaiah, V.; Ching, C. J.; Fujino, S.; Nagarajan, V.; Rabe, K. M.; Takeuchi, I.; *Adv. Funct. Mater.* **2010**, 20, 1108.

**DOI:** 10.1002/adfm.200902017

[43] B.D. Cullity, S.Stock, *Elements of X-ray Diffraction*, 3rd ed., Prentice Hall, NJ, (**2001**) p.303.

[44] Xu, J.; Wang, G.; Wang, H.; Ding, D.; He, Y.; *Mater. Lett.* **2009**, 63, 855.

**DOI:** 10.1016/j.matlet.2009.01.036

[45] Chen, J.R.; Wang, W.L.; Li, J.B.; Rao, G.H.; *J. Alloys Compd.* **2008**, 459, 66.

**DOI:**10.1016/j.jallcom.2007.05.034

[46] Khomchenko, V.A.; Shvartsman, V.V.; Borisov, P.; Kleemann, W.; Kiselev, D.A.; Bdikin, I.K.; Vieira, J.M.; Kholkin, A.L.; *J. Phys. D: Appl. Phys.* **2009**, 42, 045418.

**DOI:**10.1088/0022-3727/42/4/045418

[47] Farhadi, S.; Zaidi, M.; Mol, J.; *Catal. A: Chem.* **2009**, 299,18.

**DOI:**10.1016/j.molcata.2008.10.013

[48] Lu, J.; Yang, H.; Liu, B.; *Mater. Res. Bull.* **1999**, 34, 2109.

**DOI:** PII S0025-5408(99)00222-6

[49] Lotey, G.S.; Verma, N.K.; *Chemical Physics Letters.* **2013**, 574, 71.

**DOI:** 10.1016/j.cplett.2013.04.046

[50] Tauc, J.; Menth, A.; States in the gap. *Journal of Non-Crystalline Solids* **1972**, **8-10**, 569-85.

**DOI:** 10.1016/j.mseb.2012.03.050

[51] Palai, R.; Katiyar, R. S.; Schmid, H.; Tissot, P.; Clark, S.J.; Robertson, J.; Redfern, S.A.T.; Catalan, G.; Scott, J F.; *Phys. Rev. B* **2008**, 77,014110.

**DOI:** 10.1103/PhysRevB.77.014110

[52] Gao, F.; Chen, X.; Yin, K.; Dong, S.; Ren, Z.; Yuan, F.; Yu, T.; Zou, Z.; Liu, J.M.; *Adv. Mater.* **2007**, 19, 2889.

**DOI:** 10.1002/adma.200602377

[53] Higuchi, T.; Liu, Y.S.; Yao, P.; Glans, P.A.; Guo, J.; *Phys. Rev. B*, **2008**, 78, 085106.

**DOI:** 10.1103/PhysRevB.78.085106

[54] Wang, X.; Wang, S.Y.; Liu, W.F.; Xi, X.J.; Zhang, H.; Guo, F.; Xu, X.L.; Li, M.; Liu, L.; Zhang, C.; Li, X.; Yang, J.B.; *J Nanopart Res* **2015**, 17, 209.

**DOI:** 10.1007/s11051-015-3018-1

[55] Das, S.R.; Choudhary, R.N.P.; Bhattacharya, P.; Katiyar, R.S.; Dutta, P.; Manivannan A.; Seehra, M.S.; *J.Appl. Phys.* **2007**,101, 034104.

**DOI:** 10.1063/1.2432869

[56] Sosnowska, I.; Schafer, W.; Kockelmann, W.; Andersen, K.H.; Troyanchuk, I.O.; *Appl.Phys. A.* **2002**, 74, S1040.

**DOI:** 10.1007/s003390201604

[57] Kumar, M.; Yadav, K.L.; *J.Appl.Phys.* **2006**, 100, 074111.

**DOI:** 10.1063/1.2349491

[58] Palkar, V.R.; Kundaliya, D.C.; Malik, S.K.; Bhattacharya, S.; *Phys. Rev. B* **2004**, 69, 212102.

**DOI:** 10.1103/PhysRevB.69.212102

[59] Sundaresan, A.; Bhargavi, R.; Rangarajan, N.; Sddesh, U.; Rao, C.N.R.; *Phys. Rev. B.* **2006**, 74, 161306 (R).

**DOI:** <http://dx.doi.org/10.1103/physrevb.74.161306>

- [60] Bloembergen, N.; et al. Phys. Rev., 114.2 (**1959**): 445.
- [61] Lotey, G.S.; Verma, N.K.; Superlattices Microstruct., **2013**, 53, 184.  
**DOI:** <http://dx.doi.org/10.1016/j.cplett.2013.04.046>
- [62] Pradhan, D.K.; Choudhary, R.N.P.; Rinaldi, C.; Katiyar, R.S.;  
J Appl Phys. **2009**, 106, 024102.  
**DOI:** 10.1063/1.3158121
- [63] Prakash, D.; Masuda, Y.; Sanjeeviraja, C.; Solid State Ion. **2012**, 18, 31.  
**DOI:** 10.1007/s11581-011-0595-6
- [64] Barik, S.K.; Choudhary, R.N.P.; Singh, A.K.; Adv. Mater. Lett. **2011**, 2, 419.  
**DOI:** 10.5185/amlett.2011.2228